CARBON 75 (2014) 327–334

Available at www.sciencedirect.com

ScienceDirect

journal homepage: www.elsevier.com/locate/carbon

The role of the sp^2:sp^3 substrate content in carbon supported nanotube growth

Richard J. Cartwright [a], Santiago Esconjauregui [a,*], Robert S. Weatherup [a], David Hardeman [a], Yuzheng Guo [a], Eleanor Wright [b], Daniel Oakes [b], Stephan Hofmann [a], John Robertson [a]

[a] Department of Electrical Engineering, University of Cambridge, Cambridge CB3 0FA, United Kingdom
[b] Johnson Matthey Technology Centre, Blounts Court Road, Sonning Common, Reading RG4 9NH, United Kingdom

ARTICLE INFO

Article history:
Received 15 October 2013
Accepted 6 April 2014
Available online 13 April 2014

ABSTRACT

We report the growth of vertically-aligned nanotube forests, of up to 0.2 mm in height, on an 85:15 sp^2:sp^3 carbon support with Fe catalyst. This is achieved by purely-thermal chemical vapour deposition with the catalyst pretreated in inert environments. Pretreating the catalyst in a reducing atmosphere causes catalyst diffusion into the support and the growth of defective tubes. Other sp^2:sp^3 compositions, including graphite, tetrahedral amorphous carbon, and pure diamond, also lead to the growth of defective carbon morphologies. These results pave the way towards controlled growth of forests on carbon fibres. It could give rise to applications in enhanced fuel cell electrodes and better hierarchical carbon fibre-nanotube composites.

1. Introduction

Owing to their exceptional tensile strength and high surface area to volume ratio, carbon nanotubes (CNTs) are envisaged as nanoscale reinforcement in hierarchical carbon fibre–CNT composites [1,2], and fuel cell electrodes [3]. Two approaches have been considered for this application: (1) ex-situ growth and dispersion of nanotubes into a polymer matrix [4–7], and (2) nanotube growth by chemical vapour deposition (CVD) directly onto carbon-based materials, such as surface growth of nanotubes using fibres, yarns, or polymers as catalyst support. Direct growth is the most promising alternative, as the tubes incorporate into the composite matrix as they grow, thus forming a hierarchical structure [8–10]. In this way, the reinforcement at the nanoscale works alongside the microstructure of the fibres [11].

The surface growth of nanotubes by CVD typically involves two steps. First, the formation of catalytic nanoparticles (pretreatment), e.g. by annealing of thin film previously sputtered (or evaporated) onto an oxide support; then the growth itself, which comprises the decomposition of a gaseous carbon source followed by the nucleation of the tubes (with a diameter similar to that of the catalyst particles) [12]. CVD is a very versatile growth technique that yields tubes over a large range of temperatures and pressures. Optimised CNT CVD recipes on oxide supports (e.g. Al_2O_3 or SiO_2) lead to high nanotube purity with control over tube density, diameter, or number of walls [13–15]. However, CNT CVD directly on fibres (or other carbon-based substrates) has proved difficult to manage. The interaction between carbon-based supports and catalytic particles often leads to catalyst diffusion and/or poisoning, causing poor/defective growth [16].

* *Corresponding author.*
E-mail address: cse28@cam.ac.uk (S. Esconjauregui).
http://dx.doi.org/10.1016/j.carbon.2014.04.011

Catalyst deactivation increases with temperature, and high temperatures also deteriorate the mechanical properties of the fibres, due to damage of their surface [1,2,9]. Such effects can be minimised by reducing the CVD temperature (e.g. from 750 to ~500 °C), but the tubes grown are generally shorter, less dense, or more defective. Another alternative that has been considered is the deposition of a layer, such as Al_2O_3 or SiO_2, between the fibre and the catalyst but this affects nanotube adhesion to the support and/or the conductive properties of the fibres [17–20]. Good nanotube-fibre adhesion is a key requirement for the use of nanotubes as reinforcement, and this may be achieved if the catalyst is formed directly on the fibres; however, this is not straightforward. An intrinsic property of nanotube metal catalysts is their ability to dissolve carbon. This means the catalyst is also likely to dissolve a carbon substrate during CNT CVD, both damaging the substrate and making growth more challenging. Reducing this effect is essential for enhancing nanotube growth while protecting the carbon substrate. Here we show a promising route to achieve this goal and explain why it is feasible. We employ different types of planar carbon substrates (as an analogue to carbon fibres) on which we evaluate a wide range of CNT CVD conditions. Our results show that it is possible to obtain vertically aligned CNTs on carbon supports. We achieve nanotube forests of up to 0.2 mm in height by varying the sp^2:sp^3 ratio of the carbon support and using inert environments for Fe catalyst pretreatment. Varying the carbon–carbon bonding in the supports allows us to understand what limits nanotube growth on carbon-based materials and thus find ways to control tube properties. This work offers a promising route towards controlled growth of nanotube forests on carbon fibres. It could enable applications in enhanced fuel cell electrodes [21–23] and improved hierarchical carbon fibre–CNT composites.

2. Experimental

We evaluate nanotube growth on carbon-based supports with four different sp^2:sp^3 ratios: highly ordered pyrolytic graphite (HOPG, 100:0 sp^2:sp^3), amorphous carbon (*a*-C, 85:15 sp^2:sp^3), tetrahedral amorphous carbon (*ta*-C 30:70 sp^2:sp^3), and CVD diamond (0:100 sp^2:sp^3, pure diamond). Except for HOPG (MikroMasch®, ~0.1 mm cleaved thickness), the other supports have a nominal thickness of 100 nm and are deposited on $\sim 1 \times 1$ cm^2 polished Si wafers coated with 300 nm of SiO_2.

The *a*-C support is deposited via evaporation of a high purity carbon cord (Agar). The cord is connected and resistively heated at a base pressure of $\sim 10^{-5}$ mbar until evaporation begins; the deposition rate typically averages ~5 nm s^{-1}. The sp^3 content may vary between 15% and 30%. The *ta*-C support is deposited via a filtered cathodic vacuum arc (FCVA) system (base pressure $\sim 10^{-7}$ mbar, deposition rate ~1 Å s^{-1}) which produces a film with typically 60–80% of sp^3 carbon. CVD diamond is deposited following a previously reported technique [24].

After substrate preparation, the samples are subject to Fe catalyst deposition by thermal evaporation. We evaporate a nominally 1 nm thick, high-purity Fe (base pressure $\sim 4 \times 10^{-7}$ mbar) at an evaporation rate of ~0.1 Å s^{-1}, measured using a quartz crystal thickness monitor. The as-deposited samples are stored and transferred in air between each stage and prior to growth. All samples are pretreated in a furnace tube at 500–750 °C in 1 bar Ar (1000 sccm), i.e. inert atmosphere, or 1 bar Ar:H_2 (200:500 sccm), i.e. reducing atmosphere. In all cases, we ramp from room temperature at a nominal heating rate of 60 °C min^{-1}. Once the desired temperature is reached, the growth is carried out using Ar:H_2:C_2H_4 (200:500:500 sccm) for 10 min. The system is then left to cool under Ar atmosphere (1000 sccm) until reaching room temperature. The substrates, catalysts, and nanotubes are characterised by scanning electron microscopy (SEM) and high-resolution transmission electron microscopy (HRTEM). We use image software (ImageJ) to derive number density of catalyst particles and the weight gain method to assess the mass density of the forests [24].

In order to interpret our CNT growth results use carbon-based supports, we study the Fe–C interface by density functional theory (DFT) calculations. All calculations are done with plane wave pseudo-potential code CASTEP. We use a PBE-style generalized gradient approximation for exchanging the correlation energy and choose graphite (0001) and diamond (100) surfaces to represent pure sp^2 and pure sp^3 carbon respectively. We consider 6 layers of C (to suppress quantum confinement effects) covered with a thin layer of Fe. We use experimental values for lattice constants. The internal C atoms are fixed as the C surface is non-polar, but have previously been relaxed. Fe and top C atoms are set free to relax to a residual force of less than 3 eV Å^{-1}. As the formation energy of the Fe–C bonding depends on the choice of Fe and C chemical potential, we can compare both interfaces directly.

3. Results

Fig. 1 summarises the results for nanotube growth using the various combinations of sp^2:sp^3 carbon. All growths are performed using the same pretreatment and growth conditions. We find that the yield and morphology of the tubes are correlated to the sp^2:sp^3 ratio of the support. We find that only the 85:15 sp^2:sp^3 combination yields vertically aligned nanotube forests, as shown by side-view SEM analysis (Fig. 1(a)). At 750 °C in 1 bar Ar:H_2:C_2H_4 (200:500:500 sccm) for 10 min, the height of the forest reaches 200 ± 17 μm. The tubes are homogeneously distributed across the samples and the area density of the forest is of the order of $\sim 10^{10}$ CNTs cm^{-2}, as estimated by the weight gain method [25]. As the concentration of sp^2 carbon diminishes, the growth switches to much shorter, tangled, and completely unaligned tubes or fibres lying on the support. Fig. 1(b) shows top-view SEM images of such morphologies grown on the 30:70 sp^2:sp^3 combination. Note that as the tubes grow unaligned, cross-sectional imaging of these samples is meaningless. When the CNT CVD is performed at the two extremes of carbon bonding (HOPG and CVD diamond), nanotube growth is systematically much poorer and more difficult to control, (Fig. 1(c) and (d), respectively). We find that the nucleation can be as low as ~1 CNT μm^{-2}, regardless of the evaluated pretreatment or growth conditions. The structures produced appear to be defective fibres of only a few microns in length.

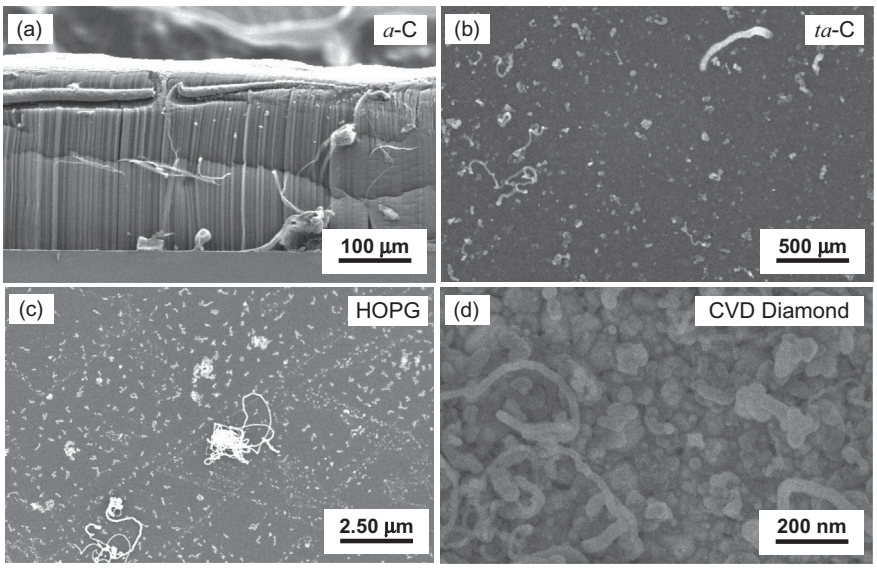

Fig. 1 – SEM images of CNTs grown on the four different sp^2:sp^3 carbon supports. The growth is performed at 750 °C in 1 bar Ar:H_2:C_2H_4 (200:500:500 sccm) for 10 m.

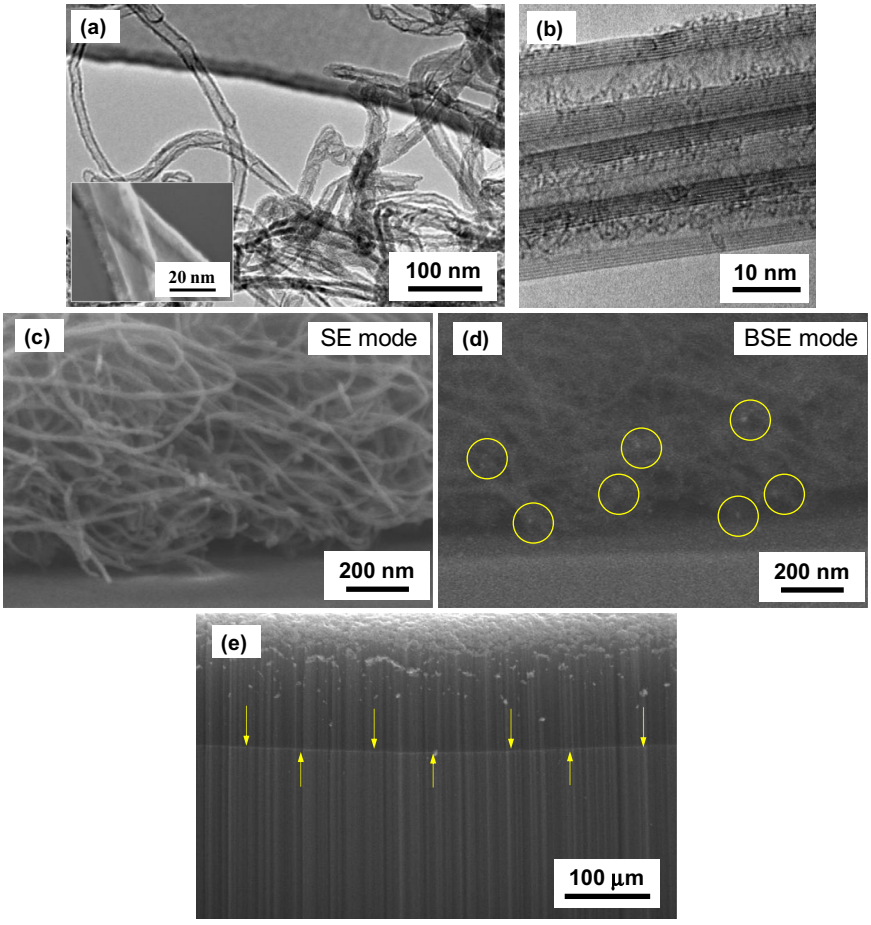

Fig. 2 – (a) and (b) TEM images of CNTs grown on *a*-C supports. (c) and (d) are respectively SE and BSE mode SEM images showing the base of forests. Nanoparticles can be easily distinguished in BSE mode (highlighted with yellow circles). (e) is a side-view SEM image of two layers of nanotubes grown by interrupted carbon source. Arrows indicate the interface. (A colour version of this figure can be viewed online.)

TEM analysis of the forests reveals multi-walled CNTs with a diameter distribution of 10–20 nm (See Fig. 2(a) and inset); accordingly, the number of walls varies from 8 to 15 (see Fig. 2(b)). No catalyst nanoparticles are identified at the tip of the tubes, suggesting a root growth mechanism. This is also suggested by SEM analysis on forests removed from the *a*-C layer and placed on a silica support. Fig. 2(c) and (d) respectively show the base of forests following removal and imaging in secondary electron and backscattered electron modes. The backscattered mode allows us to determine the presence of catalyst nanoparticles alongside the tubes, easily distinguishable from the tube carbon walls. We find the presence of Fe nanoparticles only at the base of the forests, as highlighted with yellow circles in Fig. 2(d). The growth of nanotubes by the root growth mechanism indicates a strong catalyst-support interaction. We therefore expect most particles to remain anchored to the sample following forest transfer and not to be seen by the subsequent SEM analysis. Indeed SEM inspection of the top of the forests shows no catalyst nanoparticles, further corroborating the absence of nanoparticles observed by HRTEM (Fig. 2(a) inset and (b)). We assess forest growth by the base growth mechanism using the interrupted growth method. After pretreatment, C_2H_2 is flown for 1 min, stopped for 5 min, and then on for another 10 min. This creates a two-layer array of vertically-aligned nanotube forests, as indicated by arrows in Fig. 2(e). These results not only prove the base growth mechanism, but indicate that the *a*-C/Fe interaction is overcome neither by the CNT CVD conditions, nor by the forces exerted during the formation of the graphene layers as CNTs nucleate and grow. On the other hand, HRTEM performed on the structures grown on *ta*-C, HOPG, and CVD diamond shows graphitic layers, which form compact, full-body carbon nanofibres (not shown).

The forests, tangled tubes, and other morphologies are seeded by markedly different nanoparticles. After annealing at 750 °C in 1 bar Ar (1000 sccm), the *a*-C support yields high-density nanoparticles, as shown in Fig. 3(a). SEM analysis reveals that the 1 nm Fe film restructures into nanoparticles with lateral sizes ranging 10–22 nm. Using image analysis software, we derive a nanoparticle number density of $(3.2 \pm 0.4) \times 10^{10}$ cm^{-2}, Fig. 3(a), which remains nearly invariable at 700 °C. At lower temperatures (600 or 650 °C) however, the particles appear to be larger (14–32 nm) and their number density slightly smaller ($\sim 10^{10}$ cm^{-2}). The same Fe thickness (1 nm) at 750 °C on the other carbon substrates (with different sp^2 carbon contents) yields less dense, larger nanoparticles. On HOPG the particles appear to decorate the graphitic planes (Fig. 3(b)), forming larger, less dense particles than those observed on *a*-C. In contrast, *ta*-C and CVD diamond supports show very few nanoparticles after annealing (Fig. 3(c) and (d), respectively). Both surfaces have undergone significant roughening, thus indicating Fe particles have diffused into the carbon layers. SEM imaging on backscattered electron detector shows practically no traceable metal, confirming Fe has diffused into *ta*-C and CVD diamond after pretreatment (not shown here). Nanoparticle formation on these three substrates shows no dramatic temperature dependence. At temperatures lower than 750 °C, catalyst formation (in terms of nanoparticle size and area density) is practically the same. As the CNT CVD conditions may alter the surface composition of the substrates, we have pretreated and exposed to CNT CVD the four supports prior to catalyst deposition. Following catalyst deposition, pretreatment, and growth, we observe similar growth results as on original samples. While *a*-C nucleates CNT forests, the other substrates (*ta*-C, HOPG, and CVD diamond) nucleate low-density, unaligned structures. This suggests the surface composition remains unchanged during CNT CVD. The growth results for the four substrates are summarised in Table 1.

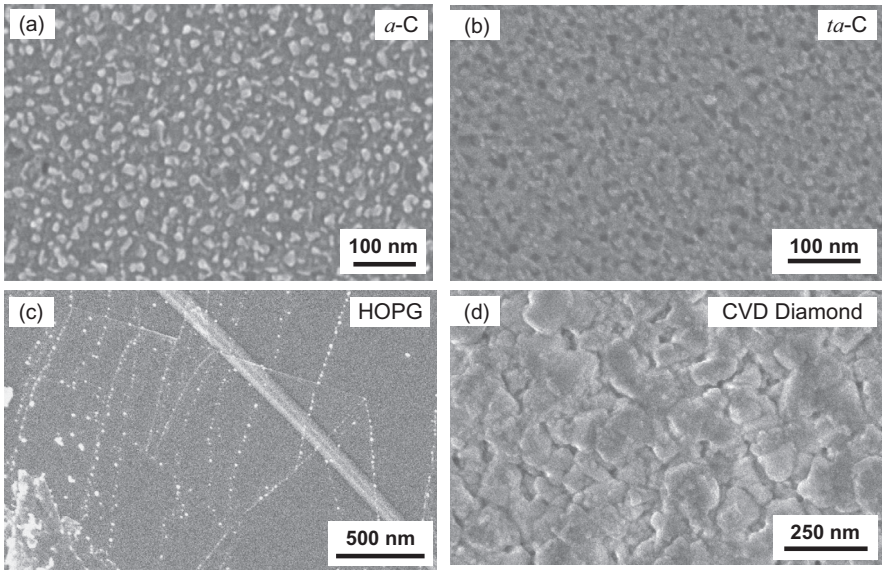

Fig. 3 – Top-view SEM images of Fe nanoparticles formed on the four different sp^2:sp^3 carbon supports. The Fe films restructure into nanoparticles following heating (a nominal heating rate of 60 °C min^{-1}) in 1 bar Ar: (1000 sccm) until reaching 750 °C.

Table 1 – CNT CVD results for the four carbon supports.

Support	sp^2:sp^3	Type of growth
HOPG	100:0	Low density, unaligned fibres
a-C	85:15	Nanotube forests
ta-C	30:70	Low density, unaligned tubes
CVD diamond	0:100	Low density, unaligned tubes

4. Discussion

4.1. *Influence of the carbon support*

The growth of CNT forests only on a particular sp^2:sp^3 carbon ratio emphasizes the influence of the support on the catalytic activity of metallic nanoparticles. This leads us to examine in detail the catalyst–support interaction for our Fe–carbon systems. The interaction is a critical parameter as it dictates the type of growth (entanglement or vertically alignment), the growth mechanism (root or tip) and, to a large extent, nanotube properties including diameter, number of walls, and length. It strongly depends on the surface and bulk properties of the support such as structure (amorphous or crystalline), roughness, or surface free energy (reactivity). In our substrates, we observe the interaction strongly depends on the carbon hybridisation rather than the surface or bulk properties of the various supports. From the four cases evaluated here, HOPG and CVD diamond are purely-crystalline carbon allotropes, while both *a*-C and *ta*-C lack any long-range order [26]. Each contains a different number of defects at the surfaces, as well as different levels of sp^1-, sp^2-, and sp^3-bonding, and thus dissimilar co-ordination numbers and chemical reactivity, which dramatically alter CNT CVD.

When the concentration of sp^3 bonds is high, as in *ta*-C, the metal catalyst–carbon interaction is strong, and nanoparticle formation and stabilisation are hard to control, as shown in Fig. 3(b). The sp^3 carbon interstitially diffuses into the metal during pretreatment, causing metal diffusion into the bulk of *ta*-C. As a result, catalyst particles are unavailable on the surface for nanotube nucleation. Likewise, pure CVD diamond is also highly susceptible to being dissolved by the metal catalyst leading to the same detrimental effects on CNT nucleation and growth (Fig. 3(c)). In the case of HOPG, however, the surface is much less reactive, so that the Fe–carbon interaction is much weaker. Fe diffusion into HOPG bulk is reduced, but Fe is highly mobile on the surface. This leads catalytic nanoparticles to strongly surface diffuse and sinter, forming inhomogeneous, large clusters along the step edges on the graphite structure (Fig. 3(b)) [27]. Note that the step edges are less chemically inert than the centres of crystalline domains. Upon exposure to a carbon source, these large particles only seed defective carbon morphologies. They are definitely unsuitable for forest growth, as indicated by Fig. 1(b).

The different Fe–carbon interactions are reflected in the energies involved when a metal dissolves HOPG or diamond. In order for a metal to dissolve sp^2 carbon, the hexagonal basal plane of the sp^2-rich support needs first to be broken. The absolute value of the bond energy of sp^2-bonded carbon is greater than that of sp^3-bonded carbon. The addition of the delocalised π electrons in graphitic carbon increases the carbon–carbon bond energy from 284–368 kJ mol^{-1} for the single -bond in sp^3 carbon to 615 kJ mol^{-1} for the double σ and π bond in sp^2 carbon [28]. This means there is a much higher energy barrier that must be overcome in order for Fe (or another metal) to decompose sp^2 carbon. Yudasaka et al. showed this for Ni [29]. They studied metal–carbon interactions via a graphitisation reaction comparing the temperature needed for a Ni film to dissolve a carbon substrate. They found the lowest energy barrier for *ta*-C, as it is more defective than pristine diamond. While for sp^2 rich carbon, and especially for pure sp^2 (graphite), the energy barrier is much larger, requiring higher temperatures for Ni to dissolve carbon (~500 °C for sp^3 carbon versus ~700 °C for sp^2 carbon).

Based on the above analysis, it is clear that both sp^2- and sp^3-rich carbon supports impose limitations for nanoparticle formation and nanotube growth. No matter which catalyst, pretreatment, or growth conditions are chosen. Formation and stabilisation of catalytically active nanoparticles on HOPG and diamond are intrinsically challenging processes. However we show here, that by selecting the ratio of sp^2 and sp^3 carbon, it is possible to obtain a carbon support suitable for the growth of forests (Fig. 1(a)). There exists an optimum sp^2:sp^3 ratio whereby nanoparticles of an appropriate size are stabilised at the catalyst surface, whilst the dissolving of carbon in the metal is minimised, as this is shown to yield defective nanotubes or nanofibres [30]. We argue this occurs for Fe nanoparticles on *a*-C and that is why our CNTs grow vertically aligned on this support. On *a*-C, the Fe nanoparticles remain anchored at the topmost surface and, following empirically optimised CVD conditions, yield forests as shown in Fig. 1(a). Conversely, on HOPG, *ta*-C, or CVD diamond, the majority of the particles either diffuse away or sinter regardless of the pretreatment or synthesis conditions evaluated, as shown in Fig. 3(b)–(d). To verify this, we have further assessed the Fe-sp^2 and Fe-sp^3 interactions at their interface by DFT calculations. Choosing graphite (0 0 0 1) and diamond (1 0 0) surfaces covered with a thin layer of Fe atoms at the surface, we observe that the interface energy per Fe atom at the diamond interface is ~7.6 eV lower than that at the graphite interface. This indicates a much stronger C–Fe bonding in sp^3 carbon than in sp^2 type, which explains the catalyst diffusion observed for *ta*-C and CVD diamond. The energy at the interface between Fe and a mix of sp^2/sp^3 carbon can then be approximated based on the composition of the carbon support. The various scenarios for nanotube growth on carbon supports are schematically shown in Fig. 4.

4.2. *Influence of the CVD conditions*

In addition to a specific sp^2:sp^3 ratio, the growth of forests on *a*-C requires the catalyst to be prepared in an inert environment. In CNT CVD on oxides, a thin film of metal catalyst is typically restructured and (simultaneously) activated into catalytically active nanoparticles by annealing in a reducing atmosphere (using H_2 or NH_3 prior to supplying the carbon source). However, on *a*-C this is not possible. Catalyst activation needs to take place during the growth period (e.g. as we have done, by supplying C_2H_4 diluted in H_2). If we anneal the catalyst films in a reducing atmosphere (e.g. Ar:H_2, 200:500 sccm), the nanoparticles diffuse into the *a*-C support.

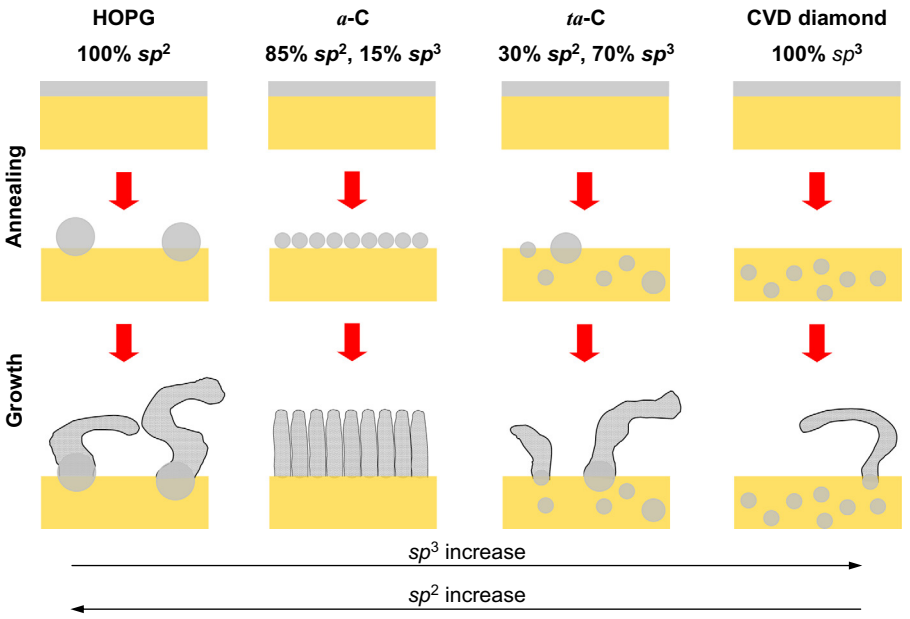

Fig. 4 – Cartoon of nanoparticle formation and nanotube growth on carbon-based supports following pure Ar catalyst pretreatment. Only a specific sp^2:sp^3 combination yields forests. (A colour version of this figure can be viewed online.)

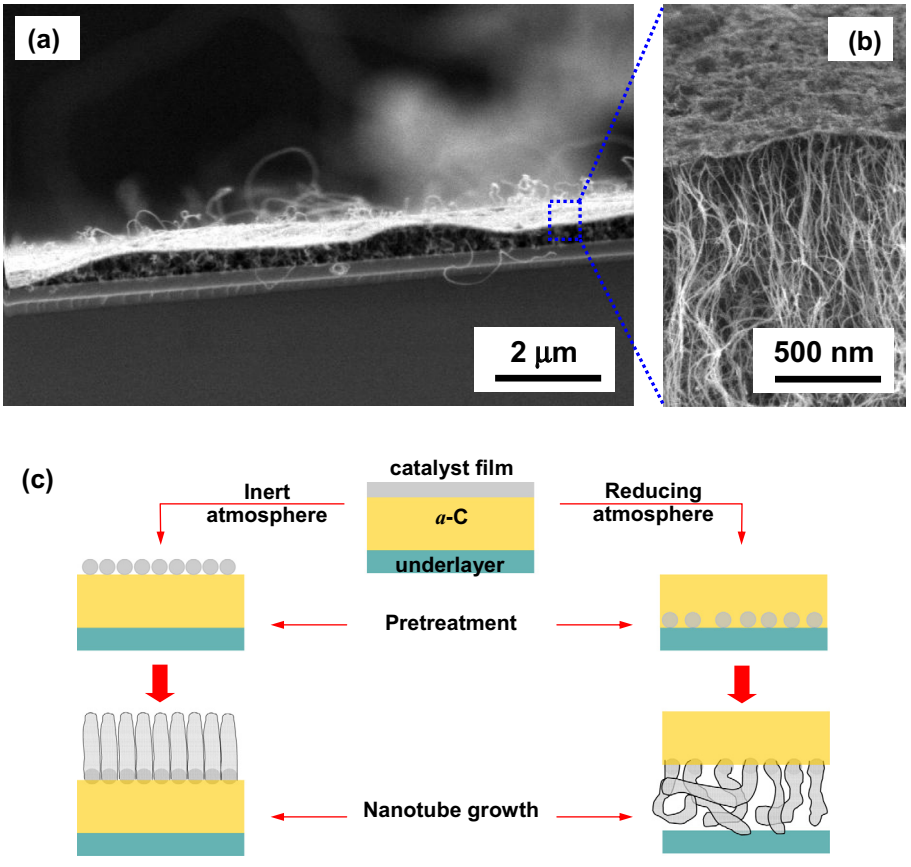

Fig. 5 – (a) and (b) are different magnification, side-view SEM images of CNT CVD on an *a*-C support following reducing catalyst pretreatment. (c) is a schematic representation of the process following either inert or reducing catalyst preparation. (A colour version of this figure can be viewed online.)

Upon supply of the carbon source, they nucleate tubes which tend to lift off the *a*-C from the silica substrate, as shown in Fig. 5(a) and (b). This is because H_2 causes a catalytic hydrogenation process, which can be likened to a reverse of the CVD reaction [31,32], typically observed on *a*-C (Fig. 5(c)).

Reverse CVD is an undesired reaction that occurs since *a*-C becomes more reactive with the catalyst under typical pretreatment/CVD conditions. The presence of H_2 during Fe annealing causes the Fe particles to catalyse the hydrogenation of carbon [31,32]. The Fe particles thus etch the *a*-C, and diffuse into the *a*-C bulk, until they reach the silica underneath (as observed on *ta*-C and diamond without a reactive atmosphere). The final particle position depends on the pretreatment time. The diffusion may be enhanced by the amorphous structure of *a*-C, compared to the parallel planes in HOPG. An inert atmosphere, however, does not favour nanoparticle formation on *ta*-C or CVD diamond. As the reactivity of sp^3 carbon is higher than that of *a*-C, the catalyst can dissolve the carbon substrate even in the absence of H_2.

Therefore by correct choice of carbon support and pretreatment atmosphere, we are able to achieve forest growth on a sp^2-rich support. This brings two immediate benefits: (1) forest growth on a non-metallic conductive support; (2) the potential for forest growth directly on carbon fibres. Fibres come in three major types: polyacrilonitrile (PAN) fibres, pitch fibres and vapour grown fibres. Fibres annealed at high temperatures to better graphitise the surface and minimise defects are more likely to give controllable nanotube growth due to higher sp^2 content and inherent resistance to being dissolved by the metal catalyst. We speculate on a process able to precisely control the graphitisation level of fibres (similar to our *a*-C 85:15 sp^2:sp^3), on which are currently working. This would allow forest growth and a good nanotube-fibre contact. Forest growth on carbon fibres could give rise to applications of enhanced fuel cell electrodes and better hierarchical carbon fibre or carbon nanotube composites. Finally, we also speculate that by a proper surface engineering of the support, catalyst design, or suitable selection of CNT CVD conditions, it might be possible to grow nanotube forests on *ta*-C, HOPG, or CVD diamond.

5. Conclusions

In conclusion, we have reviewed the effect that different types of carbon support have on the growth of CNTs. Only sp^2 rich *a*-C under selected conditions can be used to form nanoparticles suitable for nanotube forest growth. Other forms of carbon such as diamond, sp^3 rich *ta*-C and HOPG either provide a poor catalyst-substrate interaction or lead to detrimental effects on the particle and substrate. This work could lead into more controlled growth of CNTs on carbon fibres. This could in turn be used to enhance current technology in hierarchical carbon fibre-carbon nanotube composites and fuel cell electrodes.

REFERENCES

[1] Bekyarova E, Thostenson ET, Yu A, Kim H, Gao J, Tang J, et al. Multiscale carbon nanotube-carbon fiber reinforcement for advanced epoxy composites. Langmuir 2007;23(7):3970–4.

[2] Hui Q, Bismarck A, Greenhalgh ES, Shaffer MSP. Carbon nanotube grafted carbon fibres: a study of wetting and fibre fragmentation. Compos Part A: Appl Sci Manuf 2010;41(9):1107–14.

[3] Maheshwari PH, Mathur RB. Improved performance of PEM fuel cell using carbon paper electrode prepared with CNT coated carbon fibers. Electrochim Acta 2009;54(28):7476–82.

[4] Fan ZH, Hsiao KT, Advani SG. Experimental investigation of dispersion during flow of multi-walled carbon nanotube/polymer suspension in fibrous porous media. Carbon 2004;42(4):871–6.

[5] Gojny FH, Wichmann MHG, Fiedler B, Bauhofer W, Schulte K. Influence of nano-modification on the mechanical and electrical properties of conventional fibre-reinforced composites. Compos Part A: Appl Sci Manuf 2005;36(11):1525–35.

[6] Sadeghian R, Gangireddy S, Minaie B, Hsiao K-T. Manufacturing carbon nanofibers toughened polyester/glass fiber composites using vacuum assisted resin transfer molding for enhancing the mode-I delamination resistance. Compos Part A: Appl Sci Manuf 2006;37(10):1787–95.

[7] Qiu J, Zhang C, Wang B, Liang R. Carbon nanotube integrated multifunctional multiscale composites. Nanotechnology 2007;18(27):275708–18.

[8] Li WZ, Wang DZ, Yang SX, Wen JG, Ren ZF. Controlled growth of carbon nanotubes on graphite foil by chemical vapor deposition. Chem Phys Lett 2001;335(3–4):141–9.

[9] Xia Y, Zeng L, Wang W, Liang J, Lei D, Chen S, et al. Synthesis and characterization of carbon nanotubes on carbon microfibers by floating catalyst method. Appl Surf Sci 2007;253(16):6807–10.

[10] de Resende VG, Antunes EF, Lobo AdO, Lima Oliveira DA, Trava-Airoldi VJ, Corat EJ. Growth of carbon nanotube forests on carbon fibers with an amorphous silicon interface. Carbon 2010;48(12):3655–8.

[11] Hui Q, Greenhalgh ES, Shaffer MSP, Bismarck A. Carbon nanotube-based hierarchical composites: a review. J Mater Chem 2010;20(23):4751–62.

[12] Mattevi C, Wirth CT, Hofmann S, Blume R, Cantoro M, Ducati C, et al. In-situ X-ray photoelectron spectroscopy study of catalyst-support interactions and growth of carbon nanotube forests. J Phys Chem C 2008;112(32):12207–13.

[13] Hata K, Futaba DN, Mizuno K, Namai T, Yumura M, Iijima S. Water-assisted highly efficient synthesis of impurity-free single-waited carbon nanotubes. Science 2004;306(5700):1362–4.

[14] Esconjauregui S, Fouquet M, Bayer BC, Ducati C, Smajda R, Hofmann S, et al. Growth of ultrahigh density vertically aligned carbon nanotube forests for interconnects. ACS Nano 2010;4(12):7431–6.

[15] Zhong G, Warner JH, Fouquet M, Robertson AW, Chen B, Robertson J. Growth of ultrahigh density single-walled carbon nanotube forests by improved catalyst design. ACS Nano 2012;6(4):2893–903.

[16] Wirth CT, Bayer BC, Gamalski AD, Esconjauregui S, Weatherup RS, Ducati C, et al. The phase of iron catalyst nanoparticles during carbon nanotube growth. Chem Mater 2012;24(24):4633–40.

[17] Liu XM, Baronian KHR, Downard AJ. Direct growth of vertically aligned carbon nanotubes on a planar carbon substrate by thermal chemical vapour deposition. Carbon 2009;47(2):500–6.

[18] Kim B, Chung H, Kim W. Supergrowth of aligned carbon nanotubes directly on carbon papers and their properties as supercapacitors. J Phys Chem C 2010;114(35):15223–7.

[19] Li J, Srivastava S, Ok JG, Zhang Y, Bedewy M, Kotov NA, et al. Multidirectional hierarchical nanocomposites made by

carbon nanotube growth within layer-by-layer-assembled films. Chem Mater 2011;23(4):1023–31.
[20] Delmas M, Pinault M, Patel S, Porterat D, Reynaud C, Mayne-L'Hermite M. Growth of long and aligned multi-walled carbon nanotubes on carbon and metal substrates. Nanotechnology 2012;23(10):105604–11.
[21] Wang C, Waje M, Wang X, Tang JM, Haddon RC, Yan YS. Proton exchange membrane fuel cells with carbon nanotube based electrodes. Nano Lett 2004;4(2):345–8.
[22] Sun X, Li R, Stansfield B, Dodelet JP, Desilets S. 3D carbon nanotube network based on a hierarchical structure grown on carbon paper backing. Chem Phys Lett 2004;394(4–6):266–70.
[23] Hsiharng Y, Tu HC, Chiang IL. Carbon cloth based on PAN carbon fiber practicability for PEMFC applications. Int J Hydrogen Energy 2010;35(7):2791–5.
[24] Williams OA, Jackman RB. High growth rate MWPECVD of single crystal diamond. Diamond Relat Mater 2004;13(4–8):557–60.
[25] Esconjauregui S, Xie R, Fouquet M, Cartwright R, Hardeman D, Yang J, et al. Measurement of area density of vertically aligned carbon nanotube forests by the weight-gain method. J Appl Phys 2013;113:144309.
[26] Robertson J. Diamond-like amorphous carbon. Mat Sci Eng, R 2002;37(4–6):129–281.
[27] Kholmanov IN, Gavioli L, Fanetti M, Casella M, Cepek C, Mattevi C, et al. Effect of substrate surface defects on the morphology of Fe film deposited on graphite. Surf Sci 2007;601(1):188–92.
[28] Mark J. Physical properties of polymers handbook. Springer; 2007.
[29] Yudasaka M, Tasaka K, Kikuchi R, Ohki Y, Yoshimura S, Ota E. Influence of chemical bond of carbon on Ni catalyzed graphitization. J Appl Phys 1997;81(11):7623–9.
[30] Rinaldi A, Tessonnier J-P, Schuster ME, Blume R, Girgsdies F, Zhang Q, et al. Dissolved carbon controls the initial stages of nanocarbon growth. Angew Chem Int Ed 2011;50(14):3313–7.
[31] Campos LC, Manfrinato VR, Sanchez-Yamagishi JD, Kong J, Jarillo-Herrero P. Anisotropic etching and nanoribbon formation in single-layer graphene. Nano Lett 2009;9(7):2600–4.
[32] Schuenemann C, Schaeffel F, Bachmatiuk A, Queitsch U, Sparing M, Rellinghaus B, et al. Catalyst poisoning by amorphous carbon during carbon nanotube growth: fact or fiction? ACS Nano 2011;5(11):8928–34.